Journal of the Serbian Chemical Society
JSCS-info@shd.org.rs • www.shd.org.rs/JSCS

# ACCEPTED MANUSCRIPT

Journal of the Serbian Chemical Society
JSCS-info@shd.org.rs • www.shd.org.rs/JSCS
*J. Serb. Chem. Soc.* **00(0)** 1-19 (2026)
*JSCS–13845*
*Original scientific paper*
Published DD MM, 2026



# Systematic investigation into the physicochemical properties of deep eutectic $AlCl_3$/amide electrolytes with additives

CHENGYUAN LIU[1]*, CHAOYANG JIE[1], JIANGYU YU[2], YAN GUO[1], FENGCUI LI[1], SHIYAN LIU[1] AND HONGLIANG CHENG[1]

[1]*Henan University of Urban Construction, Pingdingshan 467036, China, and* [2]*School of Metallurgy, Northeastern University, Shenyang 110819, China.*

(Received 18 March; revised 4 June; accepted 21 July 2026)

*Abstract:* This study comprehensively examines the physicochemical characteristics, including density, viscosity, electrical conductivity, and electrochemical behavior, of two deep eutectic electrolytes, $AlCl_3$/acetamide and $AlCl_3$/urea, with the incorporation of various additives (LiCl, LiBr, NaCl, NaBr, EC, THF, DCE, and EMIC). The measurements were conducted across a temperature range of 313-373 K. The findings reveal that, with the exception of LiBr and NaBr, all other additives contribute to expanding the electrochemical windows of the $AlCl_3$-amide electrolytes. The addition of alkali metal halides leads to an increase in density, while EMIC and THF exert a more pronounced density-lowering effect compared to other organic additives. Inorganic additives enhance the viscosity of $AlCl_3$/acetamide but produce the opposite effect in $AlCl_3$/urea. Conversely, DCE, THF, and EMIC reduce the viscosity of both electrolytes. All investigated additives, except EC, improve electrical conductivity. Among these, EMIC demonstrates the most significant positive impact on optimizing the overall physicochemical properties of the deep eutectic $AlCl_3$/amide electrolytes.

*Keywords:* deep eutectic solvent; ionic conductivity; electrochemical window; Walden product.

## INTRODUCTION

Deep eutectic $AlCl_3$/amide electrolytes were formed by the heterolytic cleavage of $AlCl_3$ with the assistance of amides.[1-2] Owing to their adjustable acidity, high catalytic activity, cost-effectiveness, and facile preparation, these electrolytes have emerged as promising alternatives to conventional $AlCl_3$-based electrolytes.[3-4] Numerous studies have focused on the aluminum electrodeposition from $AlCl_3$/amide deep eutectic systems,[5-6] and research attention has shifted toward the structural characterization of these electrolytes,[7-10] their application as liquid

* Corresponding author. E-mail: liu_chy@126.com
https://doi.org/10.2298/JSC260318037L

catalysts,[11-14] and their use as electrolytes in aluminum-ion batteries.[15-20] However, only a limited number of studies have systematically explored the fundamental physicochemical properties, such as density, viscosity, and electrical conductivity, of $AlCl_3$/amide deep eutectic electrolytes.[10,21-22] Among the various $AlCl_3$/amide combinations, $AlCl_3$/acetamide and $AlCl_3$/urea have been the most extensively studied for applications in aluminum deposition and AIBs.

Compared to $AlCl_3$/imidazolium electrolytes, which are commonly used in aluminum-ion batteries,[23] $AlCl_3$/amide deep eutectic electrolytes suffer from narrower electrochemical stability windows, lower conductivities, and the formation of dendritic aluminum deposits during electrodeposition.[6-7] These drawbacks adversely affect the electrochemical performance of AIBs, including specific capacity, cycle stability, and operational safety. To address these issues, several studies have proposed modifying $AlCl_3$/amide electrolytes with additives, such as alkali metal chlorides, rare earth chlorides, and small organic molecules, to enhance the quality of aluminum deposits[4] and improve the electrochemical performance of aluminum-ion batteries.[18,22,24] Additionally, the physicochemical properties of certain $AlCl_3$/amide electrolytes blended with CuCl have been investigated to support the development and scaling-up of deep eutectic electrolyte-catalyzed alkylation processes.[25]

Recent studies have made significant progress in this direction. For instance, Lee *et al.* characterized the electrochemical deposition of Al from $AlCl_3$/urea containing NaCl, demonstrating that alkali metal halides can modulate plating behavior.[26] Higashino et al. revealed the long-term stability of amide-based $AlCl_3$ electrolytes under dry air, highlighting that short-term tests may overlook oxygen-induced degradation that accumulates during repeated cycling.[27] Furthermore, deep eutectic electrolytes have been successfully employed in rechargeable aluminum batteries with graphite cathodes, achieving over 8,000 cycles with a specific capacity of approximately 50 mAh $g^{-1}$ at 2 A $g^{-1}$.[28] From a fundamental perspective, the structural chemistry of $AlCl_3$/amide has been systematically investigated by combined Raman spectroscopy, NMR, and quantum chemical calculations, providing new insights into the complex speciation and hydrogen-bonding networks.[29] Guo *et al.* further developed a hypercoordinated chloroaluminate electrolyte with a chain-assisted ion transport mechanism, achieving an ionic conductivity of 0.89 mS $cm^{-1}$ and an electrochemical window exceeding 2.6 V.[30] These recent advances underscore the critical importance of understanding how additives affect electrolyte properties, yet systematic comparative studies across multiple additive types remain scarce.

In the present work, we conduct a detailed investigation into the density, viscosity, electrical conductivity, and electrochemical behavior of two $AlCl_3$/amide deep eutectic electrolytes ($AlCl_3$/acetamide and $AlCl_3$/urea) in the presence of various additives. The additives are categorized into two groups: alkali

metal halides (LiCl, LiBr, NaCl, NaBr) and organic compounds (ethylene carbonate (EC), tetrahydrofuran (THF), 1,2-dichloroethane (DCE), and 1-ethyl-3-methylimidazole chloride (EMIC)). The selection of these additives is supported by recent literature. For instance, the incorporation of NaCl into $AlCl_3$-urea DES has been shown to influence aluminum electrodeposition behavior. Meanwhile, the use of EMIC as an ionic liquid additive for chloroaluminate electrolytes has been extensively validated in solid-state AIB applications. Polar organic solvents such as EC, THF, and DCE are widely used as co-solvents in battery electrolyte engineering, as summarized in recent reviews on deep eutectic electrolytes, while EMIC is a classic imidazolium ionic liquid with excellent ionic conductivity. All additives were added at a fixed dosage of 5 mol%, which is a moderate concentration that can effectively modify electrolyte properties while avoiding phase separation and excessive viscosity increase caused by high additive content.[26,30-31]

## EXPERIMENTAL

### *Materials*

Acetamide (AcA, Sinopharm Chemical Reagent Co. Ltd., China, 99.5%), urea (Ur, Sinopharm Chemical Reagent Co. Ltd., China, 99.5%), and 1-ethyl-3-methylimidazole chloride (EMIC, Aladdin, 99%) were dried under vacuum at 333 K for 72 h. LiCl (Alfa Aesar, 99%), LiBr (Alfa Aesar, 99%), NaCl (Alfa Aesar, 99%), and NaBr (Alfa Aesar, 99%) were dried under vacuum at 393 K for 72 h. Anhydrous aluminum chloride ($AlCl_3$, Aladdin, 99%), ethylene carbonate (EC, Aladdin, 99%), tetrahydrofuran (THF, Aladdin, 99%), and 1,2-dichloroethane (DCE, Aladdin, 99%) were used without further treatment.

### *Preparation of $AlCl_3$-amide electrolyte with various additives*

$AlCl_3$/amide (amide = urea (UR), acetamide (AcA)) with a molar ratio of 1.3 was prepared by gradually adding a predetermined mass of amide into $AlCl_3$ at room temperature. Subsequently, 5 mol% of the selected additive was introduced into the liquid electrolyte, which was then stirred until a homogeneous solution was obtained. All experimental operations were performed in an argon-filled glove box (MBRAUN MB 200B, Germany) to prevent moisture and air contamination.

### *Raman spectroscopy analysis*

Raman spectra of $AlCl_3$/amide electrolyte containing additives were recorded using an HR 800 Raman spectrometer (Horiba Jobin Yvon LabRAM) equipped with a 633 nm He-Ne laser. The electrolytes were sealed in L-shaped quartz tubes to ensure stability during measurement.

### *Physicochemical behaviors measurement*

Electrochemical behavior of the $AlCl_3$/amide electrolytes (with and without additives) was evaluated using cyclic voltammetry (CV) and linear sweep voltammetry (LSV) on a tungsten working electrode at room temperature (CHI660E, Shanghai Chenhua Instrument Co., Ltd., China). The scan rates were set to 10 mV $s^{-1}$ for both cathodic and anodic processes. High-purity aluminum wire and aluminum sheet were employed as the reference and counter electrodes, respectively. Prior to use, all electrodes were polished with emery paper, cleaned with anhydrous ethanol, and dried thoroughly. The anodic limit potential ($E_{lim}$) of each electrolyte was defined as the potential where the anodic background current increased sharply during

cyclic voltammetry (CV) and linear sweep voltammetry (LSV) measurements, which corresponds to the onset of oxidative decomposition of the electrolyte system and marks the upper boundary of the electrochemical stability window.

The densities of $AlCl_3$/amide electrolytes (with and without additives) were determined via the Archimedes principle over the temperature range of 313-373 K in the glove box (MBraun GmbH, Germany). The schematic of the experimental setup is presented in Fig. S-1. Prior to liquid density measurement, the volume of the platinum sinker was firstly calibrated using anhydrous ethanol at 293 K and further verified with deionized water, yielding a volumetric measurement error below 0.1%. Given that the maximum experimental temperature was limited to 373 K, the thermal expansion of the platinum sinker was negligible. The electrolyte density was calculated using the equation (1):

$$\rho = \frac{M_1 - M_2}{V} \tag{1}$$

where, $M_1$ (g) denotes the mass of the platinum sinker before immersion into target electrolyte, $M_2$ (g) is the sinker mass after immersion, $\rho$ (g·cm$^{-3}$) refers to the density of measured liquid, and $V$ (cm$^3$) represents the pre-calibrated volume of the platinum sinker. The density of anhydrous ethanol at ambient temperature measured by this method was compared with reported literature values, with relative deviation less than 1%, which verifies the reliability of the established Archimedes-based measurement method.

Viscosities of $AlCl_3$/amide electrolytes (with and without additives) were measured by the capillary tube method inside a glove box over the temperature range of 313-373 K. As illustrated in Fig. S-2, the experimental apparatus consists of a glass capillary viscometer, stirring impeller and thermostatted oil bath. The viscosity was calculated from the efflux time required for a fixed volume of liquid to flow through the capillary under gravity. The correlation between viscosity and flow time is defined as equation (2):

$$\eta = C\rho t \tag{2}$$

where $\eta$ (mPa·s) is the viscosity of the sample electrolyte, $C$ (mm$^2$·s$^{-2}$) stands for the viscometer constant, $\rho$ (g·cm$^{-3}$) is the liquid density, and $t$ (s) denotes the recorded efflux time. To validate the measurement system, the viscosity was determined using the above setup, and the measured data agree well with previously reported literature values within acceptable experimental error, confirming the validity of the present viscosity testing approach for subsequent measurements. The temperature-dependent viscosity data were fitted to the Arrhenius equation via nonlinear least-squares regression using origin software.

Electrical conductivities of $AlCl_3$/amide electrolytes (with and without additives) were measured via the capillary impedance method in a glove box from 313 K to 373 K. The experimental setup is displayed in Fig. S-3. The electrical resistance of liquid samples was collected using an Agilent impedance analyzer (4263B LCR METER, Agilent Technologies, USA) at a fixed excitation frequency of 1000 Hz and an applied voltage of 1 V. The ionic conductivity was calculated according to equation (3):

$$\sigma = \frac{K}{R} \tag{3}$$

where $\sigma$ (mS·cm$^{-1}$) represents the conductivity of the measured electrolyte, $K$ (cm$^{-1}$) is the cell constant, and $R$ (kΩ) denotes the experimentally measured resistance of the liquid sample. The cell constant was first determined with 0.1 mol·L$^{-1}$ aqueous KCl solution and further calibrated using 1 mol·L$^{-1}$ KCl standard solution, with the resulting calibration error lower than 0.5%. The conductivity of the $AlCl_3$-EMImCl electrolyte with a molar ratio of 1.3 was measured

with the aforementioned method. The measured data were compared with literature results, and all deviations fell within acceptable experimental ranges, which verified the reliability of the present apparatus for subsequent conductivity tests. The temperature dependence of electrical conductivity was fitted to the Arrhenius equation by nonlinear least-squares fitting in origin.

## RESULTS AND DISCUSSION

### *Raman spectra*

The Raman spectra of the $AlCl_3$/amide electrolytes with various additives are presented in Fig. 1. All spectra exhibit two characteristic peaks appearing at 347 $cm^{-1}$ and 310 $cm^{-1,}$ which are assigned to the $[AlCl_4]^-$ and $[Al_2Cl_7]^-$ complexes, respectively. As reported in previous studies,[2] dynamic equilibria (4), (5), and (6) exist in $AlCl_3$/amide electrolytes. Equation (4) describes the reversible equilibrium between tetrachloroaluminate $[AlCl_4]^-$ and heptachlorodialuminate $[Al_2Cl_7]^-$. Equations (5) and (6) illustrate the mutual transformation between various aluminum-amide complex cations and anions inside the electrolytes. To assess the effect of additives on the relative content change of $[Al_2Cl_7]^-$ to $[AlCl_4]^-$ in the $AlCl_3$/amide electrolytes, the ratios of the integral area of the $[Al_2Cl_7]^-$ peak (310 $cm^{-1}$) to that of $[AlCl_4]^-$ (347 $cm^{-1}$) peak, denoted as $I_{310}/I_{347}$, were calculated (Table I). Similar Raman spectral features were reported in $AlCl_3$-N-methylformamide DES, where the $I_{310}/I_{347}$ ratio was found to be highly sensitive to the amide species and $AlCl_3$ molar ratio.[29]

$$2[AlCl_4]^- \leftrightharpoons [Al_2Cl_7]^- + Cl^- \quad (4)$$

$$[AlCl_2 \cdot 2Amide]^+ + [AlCl_4]^- \leftrightharpoons 2[AlCl_3 \cdot Amide] \quad (5)$$

$$[AlCl_2 \cdot 2Amide]^+ + [Al_2Cl_7]^- \leftrightharpoons [AlCl_3 \cdot Amide] + [Al_2Cl_6 \cdot Amide] \quad (6)$$

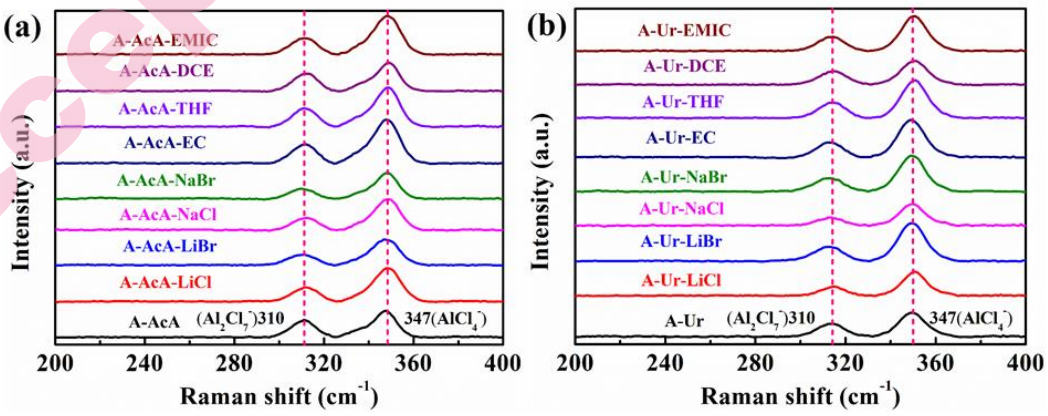


Fig. 1 Raman spectra of (a) $AlCl_3$-AcA and (b) $AlCl_3$-Ur electrolytes with various additives

TABLE I. The integral area ratio of $[Al_2Cl_7]^-$ to $[AlCl_4]^-$ ($I_{310}/I_{347}$) for $AlCl_3$/amide electrolytes containing various additives

| Additives | $I_{310}/I_{347}$ | |
|---|---|---|
| | $AlCl_3$-AcA | $AlCl_3$-Ur |
| blank | 0.65 | 0.54 |
| LiCl | 0.42 | 0.39 |
| LiBr | 0.42 | 0.36 |
| NaCl | 0.42 | 0.37 |
| NaBr | 0.41 | 0.37 |
| EC | 0.44 | 0.42 |
| THF | 0.46 | 0.42 |
| DCE | 0.66 | 0.57 |
| EMIC | 0.43 | 0.41 |

$$[Al_2Cl_7]^- + MX \leftrightharpoons [AlCl_4]^- + [AlCl_3X]^- + M^+ (M=Li, Na; X=Cl, Br) \quad (7)$$

$$[AlCl_2 \cdot x\text{Amide}]^+ + 2MX \leftrightharpoons [2M \cdot AlCl_2X_2 \cdot x\text{Amide}]^+ (M=Li, Na; X=Cl, Br) \quad (8)$$

$$[Al_2Cl_7]^- + nL \leftrightharpoons [Al_2Cl_7 \cdot nL]^- \leftrightharpoons [AlCl_4]^- + [AlCnL] (L=EC, THF, DCE) \quad (9)$$

$$[Al_2Cl_7]^- + EMIC \leftrightharpoons 2[AlCl_4]^- + EMI^+ \quad (10)$$

$$[AlCl_2 \cdot x\text{Amide}]^+ + 2EMIC \leftrightharpoons [2EMI \cdot AlCl_4 \cdot x\text{Amide}]^+ \leftrightharpoons [AlCl_4]^- + [EMI \cdot x\text{Amide}]^+ \quad (11)$$

Equations (7) and (8) depict the interactions between alkali metal halides (MX) and the intrinsic ionic species of the electrolytes. The added halide salts react with aluminum complexes and generate new halogen-containing complex ions. Equation (9) shows the complexation reaction between neutral organic additives (L) and aluminum complex anions. Organic molecules first form adducts and then decompose into different aluminum complex species. Equations (10) and (11) illustrate the reactions between EMIC and electrolyte ions. EMIC dissociates into imidazolium cations and participates in ion recombination and rearrangement. Compared to the additive-free (blank) systems, almost all additives cause a slight decrease in the relative content of $[Al_2Cl_7]^-$. This phenomenon can be attributed to chemical reactions between the additives and species in the electrolyte, as described by equations (7), (8) for inorganics, equation (9) for DCE/EC/THF, and equations (10) and (11) for EMIC. The decreasing trend of the $I_{310}/I_{347}$ ratio after adding halide salts in this work is consistent with the conclusion of NaCl-doped $AlCl_3$/urea DES, which further verifies that alkali metal halides can react with $[Al_2Cl_7]^-$ and reduce its relative content. For organic additives including THF, DCE and EC, their weak influence on the ratio of two aluminum complex ions is also in line with the structural characteristics of polar organic co-solvents in chloroaluminate electrolytes reported in previous reviews.[26]

*Electrochemical behaviors*

The electrochemical behaviors of $AlCl_3$/amide electrolytes (with and without additives) were investigated using a tungsten electrode (Fig. 2). Additives exert a

similar influence on both $AlCl_3$-AcA and $AlCl_3$-Ur electrolytes. No consistent trend was observed in the initial reduction potential ($E_0$) following the addition of additives. For the $AlCl_3$-AcA electrolytes, the initial reduction potentials ranged from -0.135 V to -0.053 V, while those of $AlCl_3$-Ur electrolytes varied between -0.126 V and -0.049 V. Distinct reduction peak in the cathodic region is assigned to the deposition of metallic aluminum, while the oxidation peak in the anodic region corresponds to aluminum stripping. The addition of additives leads to a decrease in redox current densities, which is attributed to the reduced concentration of electrochemical active species ($[Al_2Cl_7]^-$). The anodic limit potential ($E_{lim}$), defined as the potential at the sharp rise of anodic background current on voltammograms and representing the oxidative decomposition potential of electrolytes, is a critical parameter for the application of $AlCl_3$/amide electrolytes in AIBs. For both $AlCl_3$-AcA and $AlCl_3$-Ur, the addition of LiBr and NaBr shifts $E_{lim}$ to a more negative value (~1.90 V). In contrast, all other additives tend to increase $E_{lim}$, with a more pronounced effect in $AlCl_3$-Ur, where $E_{lim}$ increases from 2.23 V to approximately 2.40 V.

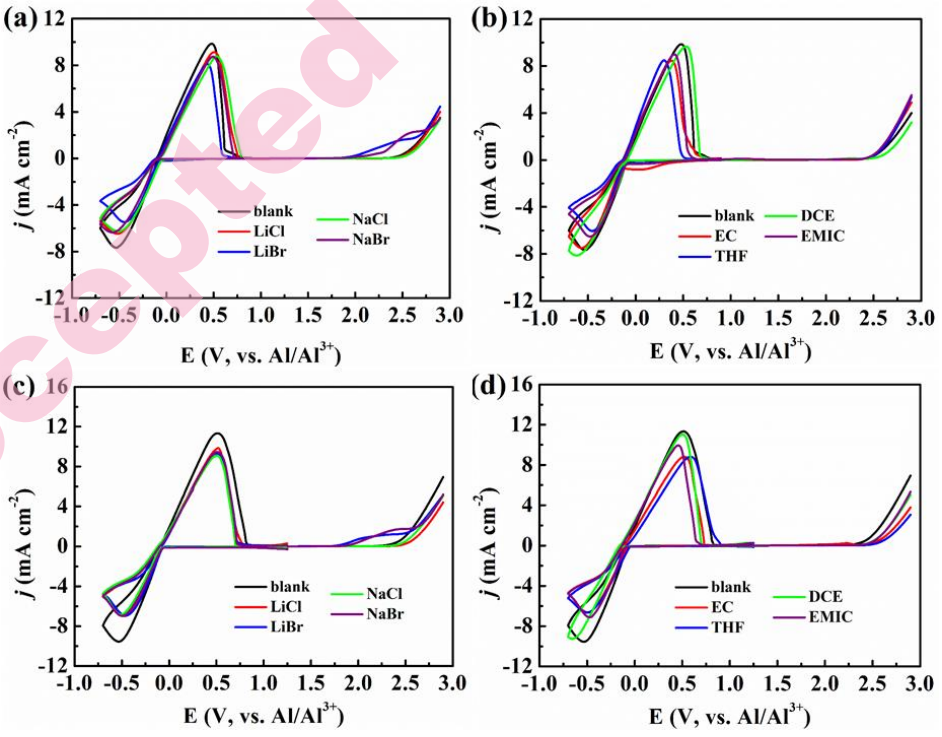


Fig. 2 Electrochemical behaviors of (a, b) $AlCl_3$-AcA and (c, d) $AlCl_3$-Ur IL analogues with various additives

The plating-stripping efficiency, defined as $\mu_{CV} = Q^+/Q^-$, was calculated to evaluate the reversibility of aluminum electrodeposition.[32] As shown in Table II, all additives improve the reversibility of aluminum deposition/stripping in both electrolytes, which is consistent with the improvement effect of alkali metal halides on aluminum electrodeposition reversibility.[26] Additionally, underpotential deposition (UPD) was observed in $AlCl_3$-AcA after the addition of EC, THF, or EMIC, a phenomenon previously reported for $AlCl_3$-EMIC electrolytes on tungsten electrodes.[33] However, UPD was not detected in any $AlCl_3$-Ur systems. This discrepancy may be associated with the unique double electric layer formed at the $AlCl_3$-Ur/W interface, as urea (with two $NH_2$ groups) exhibits stronger electrophilicity and thus a higher adsorption capacity on the electrode surface compared to acetamide.

TABLE II. The initial reduction potential ($E_0$), redox peak current densities ($j_c$ and $j_a$), anodic limit potential ($E_{lim}$), and plating-stripping efficiency ($\mu_{CV}$) obtained from the electrochemical curves in Fig. 2

| Additives | $E_0$ (V) | $j_c$ (mA cm$^{-2}$) | $j_a$ (mA cm$^{-2}$) | $E_{lim}$ (V) | $\mu_{CV}$ (%) | |
|---|---|---|---|---|---|---|
| | | | $AlCl_3$-AcA | | | |
| blank | -0.089 | -7.669 | 9.931 | 2.37 | 88.68 | |
| LiCl | -0.059 | -6.518 | 9.194 | 2.44 | 96.60 | |
| LiBr | -0.072 | -5.464 | 8.148 | 1.93 | 90.78 | |
| NaCl | -0.053 | -6.307 | 8.885 | 2.45 | 94.19 | |
| NaBr | -0.078 | -6.356 | 8.885 | 1.95 | 93.71 | |
| EC | -0.135 | -7.508 | 8.520 | 2.37 | 90.33 | UPD |
| THF | -0.102 | -6.040 | 8.520 | 2.37 | 92.08 | UPD |
| DCE | -0.083 | -8.189 | 9.721 | 2.45 | 93.30 | |
| EMIC | -0.096 | -6.567 | 9.040 | 2.37 | 94.84 | UPD |
| | | | $AlCl_3$-Ur | | | |
| blank | -0.069 | -9.502 | 11.448 | 2.23 | 91.58 | |
| LiCl | -0.075 | -6.988 | 9.875 | 2.39 | 95.64 | |
| LiBr | -0.054 | -6.932 | 9.299 | 1.85 | 98.28 | |
| NaCl | -0.088 | -6.883 | 9.145 | 2.37 | 96.16 | |
| NaBr | -0.066 | -6.988 | 9.510 | 1.87 | 94.05 | |
| EC | -0.077 | -6.616 | 8.885 | 2.40 | 94.94 | |
| THF | -0.049 | -6.721 | 8.885 | 2.42 | 95.94 | |
| DCE | -0.126 | -9.229 | 11.086 | 2.39 | 97.38 | |
| EMIC | -0.097 | -7.143 | 9.980 | 2.39 | 95.27 | |

*Density*

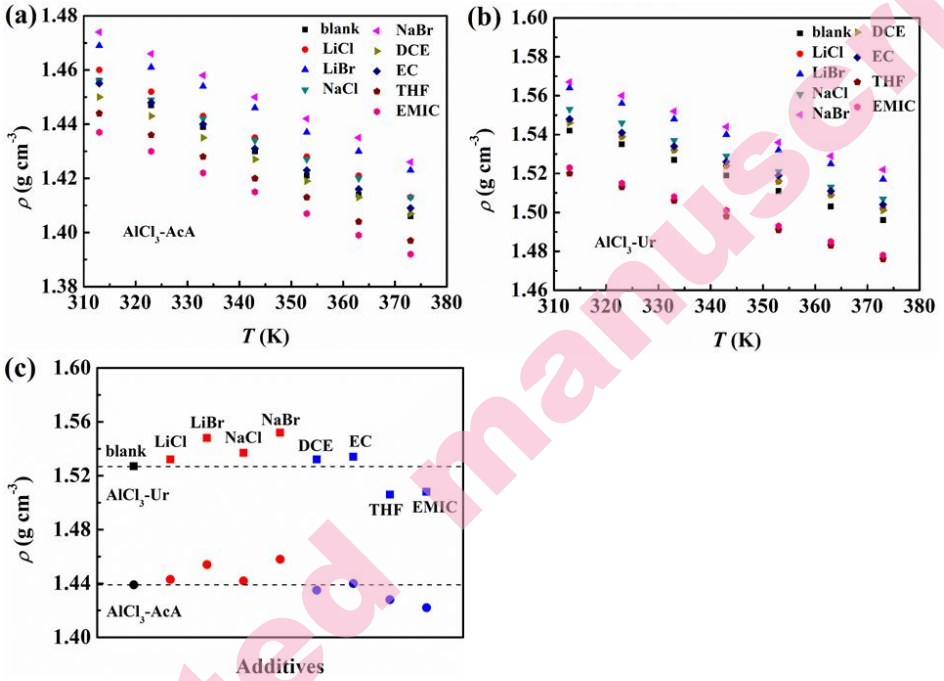


Fig. 3 Density of (a) $AlCl_3$-AcA and (b) $AlCl_3$-Ur electrolytes with various additives; (c) the density of $AlCl_3$-amide with various additives at 343 K

The density of $AlCl_3$-AcA and $AlCl_3$-Ur electrolytes with various additives is shown in Fig. 3. For all systems, density decreases linearly with increasing temperature, which can be described by the following equation:

$$\rho = a + bT \tag{12}$$

where a (g $cm^{-3}$), b (g $cm^{-3}$ $K^{-1}$) are adjustable parameters. The experimental density data and fitted parameters are provided in tables S-I and S-II. The observed temperature dependence of density is attributed to enhanced molecular vibration, weakened coulombic interactions, and increased free volume at higher temperatures. At the same temperature, the density of $AlCl_3$-AcA is lower than that of $AlCl_3$-Ur, which aligns with the density of the pure amides (AcA: 1.16 g $cm^{-3}$; Ur: 1.32 g $cm^{-3}$), suggesting that the density of the electrolytes is strongly influenced by the density of the parent amide.

As illustrated in Fig. 3(c), the addition of alkali metal halides increases the density of both $AlCl_3$-AcA and $AlCl_3$-Ur electrolytes, following the order of NaBr, LiBr > NaCl, LiCl. This indicates that the anion has a more significant impact on density than the cation. The density increase may be explained by two factors: (1) small-sized cations occupy interstitial spaces in the electrolyte, increasing the mass

per unit volume; (2) additives coordinate with anions to form species with higher densities than the original $AlCl_3$/amide complexes. Additionally, reactions between additives and electrolyte species reduce the average pore radius, further contributing to a slight density increase. For organic additives, the effect on density follows the order: EC > DCE ≥ blank > THF, which matches the density order of the pure organic compounds. EMIC causes a significant decrease in density due to its large imidazolium cation, which increases free volume and reduces the concentration of species per unit volume. Raman spectroscopy results further confirm that EMIC addition decreases the concentration of the heavier $[Al_2Cl_7]^-$ anion, which also contributes to the density reduction. The density-increasing effect of alkali metal halides observed here is consistent with the findings that a density increase upon NaCl addition to $AlCl_3$-urea DES.[26] Furthermore, recent studies on other DES systems have similarly reported that the addition of lithium salts tends to increase density while decreasing free volume, in agreement with the present results.[34]

*Viscosity*

Viscosity data for $AlCl_3$/amide electrolytes with various additives are presented in table S-III, and the temperature dependence of viscosity is shown in Fig. 4(a) and Fig. 4(b). Viscosity follows an Arrhenius relationship with temperature:

$$\eta = \eta_0 \, exp(-E_\eta/RT) \tag{13}$$

where $\eta_0$ (mPa s) and $E_\eta$ (kJ mol$^{-1}$) are empirical constants. Fitted parameters are listed in table III. All fitting results show high $R^2$ values (>0.99), confirming the excellent correlation between viscosity and temperature following the Arrhenius rule. The apparent activation energy $E_\eta$ for viscosity reflects the energy barrier for ion and molecular migration. For both electrolytes, EMIC, THF and DCE present lower $E_\eta$ values than blank samples, indicating reduced flow resistance. In contrast, EC gives a much higher activation energy, which is consistent with its viscosity-increasing effect. The fitted pre-exponential factor $\eta_0$ also varies with the type of additives, further proving the regulation effect of additives on the fluidity of the electrolytes.

The viscosity of deep eutectic electrolytes is influenced by factors such as hydrogen bond network between each component, ion size, void volume, intermolecular forces (e.g., electrostatic and van der Waals interactions).[35] As shown in Fig. 4(a, b), the viscosity of each electrolyte decreases sharply with increasing temperature, suggesting that the increase of temperature significantly reduces the polymerization energy and hydrogen bonds among the species in liquids. On the other hand, increased free volume results in an easy movement of ions into vacant sites.[36]

TABLE III. Arrhenius equation fitting parameters of viscosity and temperature for $AlCl_3$-AcA and $AlCl_3$-Ur electrolytes with various additives

| Additives | $\eta = \eta_0 \exp(-E_\eta/RT)$ | | |
|---|---|---|---|
| | $\eta_0$ | $E_\eta$ | $R^2$ |
| | $AlCl_3$-AcA | | |
| blank | 0.00065 | 28.975 | 0.9906 |
| LiCl | 0.00055 | 29.382 | 0.9928 |
| LiBr | 0.00114 | 27.592 | 0.9973 |
| NaCl | 0.00118 | 27.418 | 0.9975 |
| NaBr | 0.00102 | 27.937 | 0.9975 |
| DCE | 0.00138 | 26.766 | 0.9960 |
| EC | 0.00118 | 27.490 | 0.9976 |
| THF | 0.00132 | 26.898 | 0.9971 |
| EMIC | 0.00131 | 26.732 | 0.9973 |
| | $AlCl_3$-Ur | | |
| blank | 0.00113 | 27.750 | 0.9971 |
| LiCl | 0.00108 | 27.619 | 0.9974 |
| LiBr | 0.00133 | 27.239 | 0.9963 |
| NaCl | 0.00096 | 28.266 | 0.9970 |
| NaBr | 0.00099 | 28.109 | 0.9952 |
| DCE | 0.00214 | 25.591 | 0.9926 |
| EC | 0.00017 | 33.612 | 0.9952 |
| THF | 0.00132 | 27.140 | 0.9970 |
| EMIC | 0.00179 | 25.954 | 0.9954 |

The effect of additives on viscosity of $AlCl_3$/amide electrolytes was analyzed by comparing values at 343 K (Fig. 4(c) and Fig. 4(d)). For $AlCl_3$-AcA, alkali metal halides increase viscosity. This is because the addition of these salts increases the relative molecular mass of the electrolyte, enhancing van der Waals forces,[25] and reduces void volume, thereby decreasing the mobility of free species.[35] In contrast, DCE, THF, and EMIC reduce the viscosity of $AlCl_3$-AcA by solvating constituent ions and reducing ion aggregation.[37-38] EMIC exhibits a more pronounced viscosity-lowering effect than DCE or THF, as its large cation increases void volume in the electrolyte. Notably, EC increases the viscosity of $AlCl_3$-AcA, likely due to the formation of an extensive hydrogen-bond network between the three oxygen atoms in EC and species in the electrolyte. For $AlCl_3$-Ur, organic additives exert a similar effect on viscosity as observed in $AlCl_3$-AcA. However, alkali metal halides decrease the viscosity of $AlCl_3$-Ur, an opposite trend to that in $AlCl_3$-AcA. This difference arises from the stronger 3D hydrogen-bond network in $AlCl_3$-Ur, which is formed by the two $NH_2$ groups in urea (compared to one in acetamide). The addition of alkali metal halides partially disrupts this network, which becomes the dominant factor overriding other force-enhancing effects, leading to a net decrease in viscosity. The viscosity-reducing effect of

organic additives observed here aligns with the findings of the FNMA-LiTFSI DES system, where the incorporation of small organic molecules was shown to significantly reduce viscosity while enhancing ionic conductivity.[34] Meanwhile, the inverse effect of alkali metal halides in $AlCl_3$-AcA versus $AlCl_3$-Ur is reminiscent of the composition-dependent viscosity behavior reported in EMIC-$AlCl_3$ systems with varying Lewis acidity.[39]

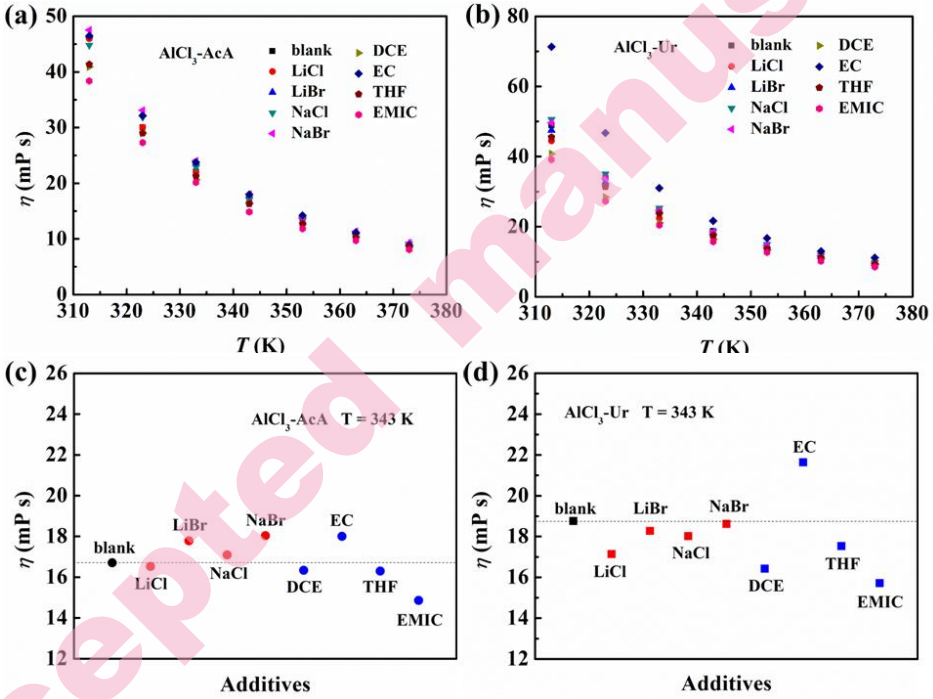


Fig. 4 Temperature dependence on the viscosity of (a) $AlCl_3$-AcA and (b) $AlCl_3$-Ur electrolytes with various additives; the viscosity of (c) $AlCl_3$-AcA and (d) $AlCl_3$-Ur electrolytes with various additives at 343 K

*Electrical conductivity*

The electrical conductivities of $AlCl_3$-amide electrolytes with various additives are listed in table S-IV. The temperature dependency of electrical conductivity is shown in Fig. 5. As expected, the electrical conductivities increase with temperature for all $AlCl_3$-amide electrolytes, as higher temperatures weaken intermolecular interactions, increase average pore radius, and enhance ion mobility. The experimental data have been fitted by the Arrhenius equation:

$$\sigma = \sigma_0 \, exp(-E_\sigma/RT) \tag{14}$$

where $\sigma_0$ (S·cm$^{-1}$) and $E_\sigma$ (kJ mol$^{-1}$) are adjustable parameters. The values of best fitted parameters are presented in table IV. The electrical conductivity data

were well fitted by the Arrhenius equation with all $R^2 > 0.99$. The activation energy $E_\sigma$ for ionic migration represents the energy required for ion transport. It is found that EMIC delivers the lowest $E_\sigma$ among all additives, which explains its optimal conductivity improvement. Most inorganic halides show moderate $E_\sigma$ values, while EC corresponds to a relatively higher migration barrier, leading to its negative effect on conductivity.

As shown in Figs. 5(c) and 5(d), all additives except EC improve the electrical conductivity of both $AlCl_3$/amide electrolytes. For organic additives (DCE, THF, EMIC), the change of conductivity has the inverse proportion to the viscosity, which indicates that weakened intermolecular interactions and enhanced ion mobility are the primary drivers of conductivity improvement. Furthermore, EMIC exhibits the most significant conductivity-enhancing effect among organic additives, which is attributed to its ionic liquid nature (unlike molecular DCE and THF). Alkali metal halides also increase electrical conductivity of $AlCl_3$-AcA and $AlCl_3$-Ur electrolytes, but through a different mechanism. The addition of these salts increases the concentration of small, highly mobile ions ($Li^+$ and $Na^+$), which migrate more easily between free volume than large complex species in the electrolyte, thereby improving overall conductivity.

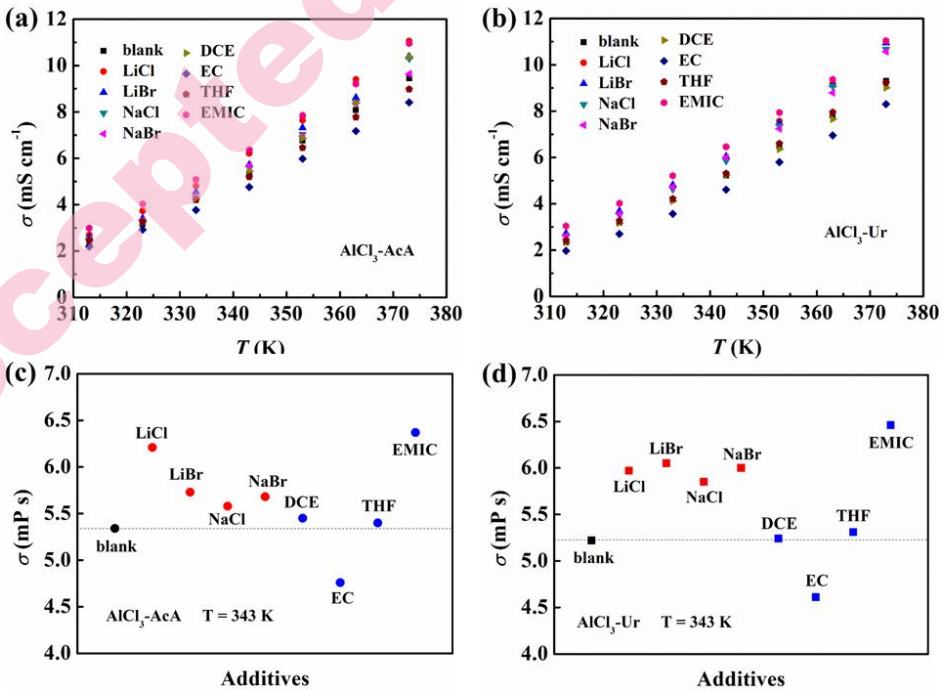


Fig. 5 Temperature dependence on the conductivity of (a) $AlCl_3$-AcA and (b) $AlCl_3$-Ur electrolytes with various additives; the conductivity of (c) $AlCl_3$-AcA and (d) $AlCl_3$-Ur electrolytes with various additives at 343 K

TABLE IV. Arrhenius equation fitting parameters of conductivity and temperature for $AlCl_3$-AcA and $AlCl_3$-Ur electrolytes with various additives

| Additives | $\sigma = \sigma_0 \exp(-E_\sigma/RT)$ | | |
|---|---|---|---|
| | $10^4\sigma_0$ | $E_\sigma$ | $R^2$ |
| | $AlCl_3$-AcA | | |
| blank | 1.5651 | 22.796 | 0.9970 |
| LiCl | 1.7957 | 22.783 | 0.9986 |
| LiBr | 1.4901 | 22.444 | 0.9958 |
| NaCl | 1.6354 | 22.811 | 0.9975 |
| NaBr | 1.3631 | 22.280 | 0.9967 |
| DCE | 1.6957 | 22.951 | 0.9993 |
| EC | 1.0741 | 22.036 | 0.9987 |
| THF | 0.8980 | 21.262 | 0.9991 |
| EMIC | 0.8506 | 20.562 | 0.9967 |
| | $AlCl_3$-Ur | | |
| blank | 0.9189 | 21.347 | 0.9978 |
| LiCl | 1.4994 | 22.339 | 0.9986 |
| LiBr | 1.2155 | 21.722 | 0.9990 |
| NaCl | 1.3696 | 22.144 | 0.9976 |
| NaBr | 1.0820 | 21.471 | 0.9975 |
| DCE | 0.7415 | 20.772 | 0.9967 |
| EC | 1.0827 | 22.198 | 0.9972 |
| THF | 0.7631 | 20.772 | 0.9964 |
| EMIC | 0.7131 | 20.028 | 0.9961 |

Molar conductivity ($\Lambda$) is a key parameter for evaluating ion mobility. Based on electrical conductivity and density values, the molar conductivities of $AlCl_3$/amide electrolytes with various additives have been calculated by the following equation:

$$\Lambda = \frac{\sigma M}{\rho} \tag{15}$$

where $M$ represents the molar mass of $AlCl_3$/amide electrolytes. The data of molar conductivity are provided in table S-V, and the temperature dependence of molar conductivity ($\Lambda$) is shown in Fig. 6(a) and (b). As observed for electrical conductivity, molar conductivity increases with temperature and is improved by all additives except EC (Figs. 6(c) and 6(d)). This confirms that smaller charge carriers and larger void volume are beneficial for electrolyte conductivity.

To further assess ionic transport efficiency, Walden plots were constructed by plotting $\log(\Lambda)$ against $\log(\eta^{-1})$ (Fig. 7). The Walden product ($\Lambda\eta=k$) is a

temperature-dependent constant that reflects the degree of ion dissociation or iconicity of a liquid. A dilute 0.01 M KCl solution, where ions are fully dissociated and exhibit equal mobility, was used as a reference. “Good ionic liquids” lie near the ideal KCl line, while those above the line are classified as “superionic” and those below as “poor ionic liquids” (characterized by significant cation-anion pairing or correlated ion motion).[40-41]

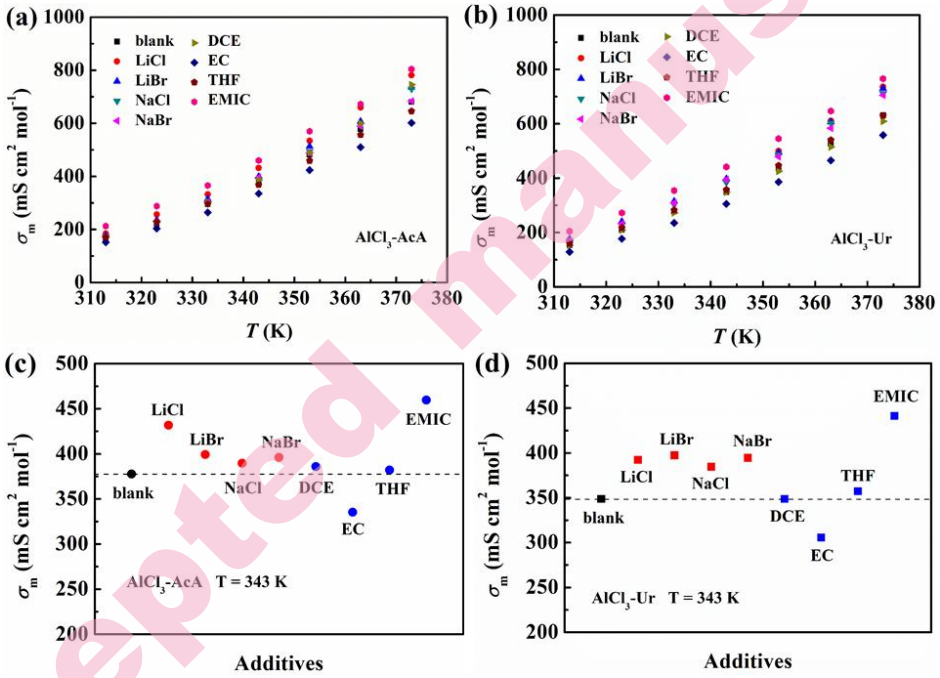


Fig. 6 Temperature dependence on the molar conductivity of (a) $AlCl_3$-AcA and (b) $AlCl_3$-Ur electrolytes with various additives; the molar conductivity of (c) $AlCl_3$-AcA and (d) $AlCl_3$-Ur electrolytes with various additives at 343 K

As shown in Fig. 7, All $AlCl_3$/amide electrolytes fall into the “poor ionic liquids” classification region. In contrast, $AlCl_3$-EMIC ionic liquids model behavior lies near the ideal KCl line on the Walden plot and is classified as a “true ionic liquid”. Notably, All $AlCl_3$/amide electrolytes deviate from the ideal KCl line by less than 20%, indicating a high degree of ion association and classification as “associated ionic liquids”, an intermediate between true ionic liquids and molecular species.[41] For instance, the FNMA-LiTFSI DES was shown to exhibit vehicular transport as the main ion transport mechanism, with a strong coupling between ionic conductivity and viscous flow.[34] The present Walden plot results further support that all investigated additives maintain the associated ionic liquid character while improving ionic conduction efficiency. As will be discussed

shortly, the aluminum species in $AlCl_3$/amide electrolytes are chemically separated, and there is some coordination between the cation and anion mobility. This also accounts for the lower conductivity of $AlCl_3$/amide deep eutectic electrolytes compared to $AlCl_3$-EMIC ionic liquid. The Walden product provides a valuable benchmark for selecting additives to enhance the ionic conduction efficiency of electrolytes in future studies.

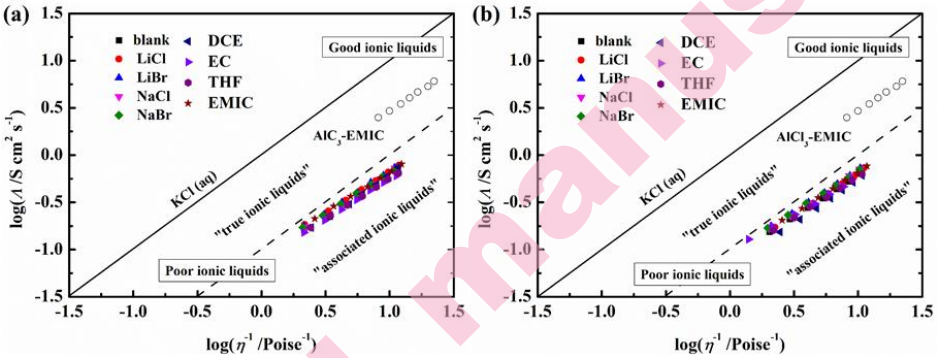


Fig. 7 Walden plot for (a) $AlCl_3$-AcA and (b) $AlCl_3$-Ur electrolytes with various additives

## CONCLUSION

This study systematically investigates the density, viscosity, electrical conductivity, and electrochemical behavior of $AlCl_3$-AcA and $AlCl_3$-Ur deep eutectic electrolytes with eight additives (LiCl, LiBr, NaCl, NaBr, EC, THF, DCE, EMIC) over a temperature range of 313-373 K. The key findings are as follows: All additives improve the reversibility of aluminum deposition/stripping in both electrolytes. Except for LiBr and NaBr, all additives expand the electrochemical windows of the $AlCl_3$/amide electrolytes. Alkali metal halides increase electrolyte density, while EMIC and THF produce the most significant density-lowering effect among organic additives. Inorganic additives increase the viscosity of $AlCl_3$-AcA but decrease that of $AlCl_3$-Ur; DCE, THF, and EMIC reduce the viscosity of both electrolytes. All additives except EC enhance electrical conductivity, with EMIC exhibiting the most pronounced effect on reducing viscosity and increasing conductivity. These results provide valuable insights for optimizing $AlCl_3$/amide deep eutectic electrolytes for applications in AIBs and catalytic processes.

## SUPPLEMENTARY MATERIAL

Additional data are available electronically at the pages of journal website: https://www.shd-pub.org.rs/index.php/JSCS/article/view/13845, or from the corresponding author on request.

*Acknowledgements:* This work was supported by the Natural Science Foundation of Henan Province of China (252300420759), the Key Scientific Research Project of Colleges and

Universities in Henan Province (26B630005), Henan Key Science and Technology Research (262102230097), and Henan University of Urban Construction Young Backbone Teacher Training Program (YCJQNGGJS202507, YCJQNGGJS202503).

## ИЗВОД

### СИСТЕМАТСКО ИСПИТИВАЊЕ ФИЗИЧКОХЕМИЈСКИХ СВОЈСТАВА ДУБОКИХ ЕУТЕКТИЧКИХ $AlCl_3$/АМИДНИХ ЕЛЕКТРОЛИТА СА АДИТИВИМА

CHENGYUAN LIU[1*], CHAOYANG JIE[1], JIANGYU YU[2], YAN GUO[1], FENGCUI LI[1], SHIYAN LIU[1] AND HONGLIANG CHENG[1]

*[1]Henan University of Urban Construction, Pingdingshan 467036, China, and [2]School of Metallurgy, Northeastern University, Shenyang 110819, China.*

Ова студија представља свеобухватно испитивање физичкохемијских карактеристика, укључујући густину, вискозност, електричну проводљивост и електрохемијско понашање, два дубока еутектичка електролита, $AlCl_3$/ацетамид и $AlCl_3$/уреа, уз уградњу различитих адитива (LiCl, LiBr, NaCl, NaBr, EC, THF, DCE и EMIC). Мерења су спроведена у температурном опсегу од 313 до 373 K. Добијени резултати показују да, са изузетком LiBr и NaBr, сви остали адитиви доприносе проширењу електрохемијских опсега $AlCl_3$/амидних електролита. Додатак халогенида алкалних метала доводи до повећања густине, док EMIC и THF показују израженији ефекат смањења густине у поређењу са другим органским адитивима. Неоргански адитиви повећавају вискозност $AlCl_3$/ацетамида, али производе супротан ефекат код $AlCl_3$/урее. Насупрот томе, DCE, THF и EMIC смањују вискозност оба електролита. Сви испитани адитиви, осим EC, побољшавају електричну проводљивост. Међу њима, EMIC показује најзначајнији позитиван утицај на оптимизацију укупних физичкохемијских својстава дубоких еутектичких $AlCl_3$/амидних електролита.

(Примљено 18. марта; ревидирано 4. јуна; прихваћено 21. јула 2026.)

## REFERENCES

1. H. M. A. Abood, A. P. Abbott, A. D. Ballantyne, K. S. Ryder, *Chem. Commun.* **47** (2011) 3523 (https://doi.org/10.1039/C0CC04989A)
2. F. Coleman, G. Srinivasan, M. S. Kwaśny, *Angew. Chem.* **52** (2013) 12582 (https://doi.org/10.1002/anie.201306267)
3. J. Wang, *Tailoring Electrolytes for Extreme Temperatures in Rechargeable Aluminum and Lithium-Ion Batteries*, PhD Thesis, CUNY City College, CUNY Academic Works (2025) (https://academicworks.cuny.edu/cc_etds_theses/1259)
4. A. Zobeid, F. Abbasi, S. Azadi, *Adv. Appl. NanoBio Tech.* **6** (2025) 18615 (https://doi.org/10.18502/AANBT.V6I2.18615)
5. V. S. Cvetković, N. M. Vukićević, N. Jovićević, J. S. Stevanović, J. N. Jovićević, *Trans. Nonferrous Met. Soc. China* **30** (2020) 823 (https://doi.org/10.1016/S1003-6326(20)65257-8)
6. S. Prabu, H. W. Wang, *Chinese J. Chem. Eng.* **28** (2020) 854 (https://doi.org/10.1016/j.cjche.2019.11.002)
7. P. C. Hu, R. Zhang, X. H. Meng, H. Y. Liu, C. M. Xu, Z. C. Liu, *Inorg. Chem.* **55** (2016) 2374 (https://doi.org/10.1021/acs.inorgchem.5b02744)

8. P. C. Hu, W. Jiang, L. J. Zhong, S. F Zhou, *RSC Adv.* **8** (2018) 13248 (https://doi.org/10.1039/C8RA01845F)
9. M. Malik, K. L. Ng, G. Azimi, *Electrochim. Acta* **354** (2020) 136708 (https://doi.org/10.1016/j.electacta.2020.136708)
10. Y. Liu, R. S. Hu, C. M. Xu, H. Q. Su, *Appl. Catal. A-Gen.* **346** (2008) 189 (https://doi.org/10.1016/j.apcata.2008.05.024)
11. J. M. Hogg, F. Coleman, A. F. Ugalde, M. P. Atkins, M. S. Kwaśny, *Green Chem.* **17** (2015) 1831 (https://doi.org/10.1039/C4GC02080D)
12. P. C. Hu, Y. D. Wang, X. H. Meng, R. Zhang, H. Y. Liu, C. M. Xu, Z. C. Liu, *Fuel* **189** (2017) 203 (https://doi.org/10.1016/j.fuel.2016.10.099)
13. P. C. Hu, J. W. Zheng, W. Jiang, L. J. Zhong, S. F. Zhou, *Chinese J. Chem. Eng.* **28** (2020) 152 (https://doi.org/10.1016/j.cjche.2019.04.018)
14. K. Matuszek, A. Chrobok, J. M. Hogg, F. Colemanb, M. S. Kwaśny, *Green Chem.* **17** (2015) 4255 (https://doi.org/10.1039/C5GC00749F)
15. M. Angell, C. J. Pan, Y. M. Rong, C. Z. Yuan, M. C. Lin, B. J. Hwang, H. J. Dai, *PNAS* **114** (2017) 834 (https://doi.org/10.1073/pnas.1619795114)
16. Y. T. Kao, S. B. Patil, C. Y. An, S. K. Huang, J. C. Lin, T. S. Lee, Y. C. Lee, H. L. Chou, C. W. Chen, Y. J. Chang, Y. H. Lai, D. Y. Wang, *ACS Appl. Mater. Interfaces* **12** (2020) 25853 (https://doi.org/10.1021/acsami.0c04640)
17. X. Y. Bao, Z. S. Wang, D. Zhang, R. Y. Hong, M .L. Li, C. M. Smithc, J. J. Xu, *New J. Chem.* **48** (2024) 5893 (https://doi.org/10.1039/d4nj00147h)
18. N. Canever, N. Bertrand, T. Nann, *Chem. Commun.* **54** (2018) 11725 (https://doi.org/10.1039/C8CC04468F)
19. C. Xu, T. Diemant, X. Liu, S. Passerini, *Adv. Mater.* **36** (2024) 2400263 (https://doi.org/10.1002/adma.202400263)
20. M. Raić, O. Lužanin, I. Jerman, R. Dominko, J. Bitenc, *J. Power Sources* **624** (2024) 235575 (https://doi.org/10.1016/j.jpowsour.2024.235575)
21. M. Angell, G. Z. Zhu, M. C Lin, Y. M. Rong, H. J. Dai, *Adv. Funct. Mater.* **30** (2019) 1901928 (https://doi.org/10.1002/adfm.201901928)
22. J. F. Li, J.G. Tu, H. D. Jiao, C. Wang, S. Q. Jiao, *J. Electrochem. Soc.* **164** (2017) A3093 (https://doi.org/10.1149/2.0811713jes)
23. K. V. Kravchyk, M. V. Kovalenko, *Commun. Chem.* **3** (2020) 120 (https://doi.org/10.1038/s42004-020-00365-2)
24. F. C. Li, C. Y. Liu, R. J. Liu, J. Y. Yu, Z. W. Liu, *Electrochemistry* **91** (2023) 057005 (https://doi.org/10.5796/electrochemistry.23-00028)
25. P. C. Hu, W. Jiang, L. J. Zhong, S. F. Zhou, *Chinese J. Chem. Eng.* **27** (2019) 144 (https://doi.org/10.1016/j.cjche.2018.06.018)
26. J. Lee, Y.R. Gwon, S. Kim, J. Lee, S. Choe, P.K. Song, B. Yoo, *J. Appl. Electrochem.* **55** (2025) 2999 (https://doi.org/10.1007/s10800-025-02356-4)
27. S. Higashino, T. Yamamoto, T. Ikenoue, T. Hirato, M. Miyake, *J. Electrochem. Soc.* **173** (2026) 112503 (https://doi.org/10.1149/1945-7111/ae7476)
28. F. Jach, M. Wassner, M. Bamberg, E. Brendler, G. Frisch, U. Wunderwald, J. Friedrich, *ChemElectroChem* **8** (2021) 1988 (https://doi.org/10.1002/celc.202100183)
29. Q. L. Meng, X. W. Hu, R. D. Guo, A. M. Liu, J. Y. Yu, Z. N. Shi, Z. W. Wang. *Inorg. Chem.* **64** (2025) 17722 (https://doi.org/10.1021/acs.inorgchem.5c01791)
30. K. Guo, W. Wang, H. D. Jiao, W. L. Song, S. Q. Jiao, *ACS Nano* **19** (2025) 32595 (https://doi.org/10.1021/acsnano.5c09979)

31. D. C. Wu, X. L. Wang, S. J. Yang, Y. H. Zhu, Z. H. Zuo, Z. Liao, J. Liu, H. Yuan, J. Q. Huang, *Adv. Sci.* **13** (2026): e17939 (https://doi.org/10.1002/advs.202517939)
32. M. Torrero, P. Leung, E. G. Quismondo, E. Ventosa, M. Anderson, J. Palma, R. Marcilla, *J. Power Sources* **374** (2018) 77 (https://doi.org/10.1016/j.jpowsour.2017.11.032)
33. T. Jiang, M. J. C. Brym, G. Dubé, A. Lasia, G. M. Brisard, *Surf. Coat. Tech.* **201** (2006) 1 (https://doi.org/10.1016/j.surfcoat.2005.10.046)
34. G. Lyu, C. Korte, J. Luo, *Materials* **18** (2025) 2048 (https://doi.org/10.3390/ma18092048)
35. Q. H. Zhang, K. D. O. Vigier, S. Royer, F. Jérôme, *Chem. Soc. Rev.* **41** (2012) 7108 (https://doi.org/10.1039/C2CS35178A)
36. R. L. Perry, K. M. Jones, W. D. Scott, Q. Liao, C. L. Hussey, *J. Chem. Eng. Data* **40** (1995) 615 (https://doi.org/10.1021/je00019a017)
37. Y. Z. Jia, *Ionic liquid analogues*, Chemical Industry Press, Beijing, China, 2015 (ISBN 978-7-122-22060-8)
38. A. García, L. C. T. González, K. P. Padmasree, M. G. B. Garcia, E. M. Sánchez, *J. Molecular Liq.* **178** (2013) 57 (https://doi.org/10.1016/j.molliq.2012.11.007)
39. K. Venkatesh, A. Ispas, A. Bund, *Meet. Abstr.* **MA2025-01** (2025) 1406 (https://doi.org/10.1149/MA2025-01231406mtgabs)
40. R. E. Ramírez, L. C. T. González, A. Hernández, A. García, E. M. Sánchez, *J. Phys. Chem. B* **114** (2010) 4271 (https://doi.org/10.1021/jp910706m)
41. D. R. MacFarlane, M. Forsyth, E. I. Izgorodina, A. P. Abbott, G. Annata, K. Fraser, *Phys. Chem. Chem. Phys.* **11** (2009) 4962 (https://doi.org/10.1039/B900201D).